

Plate generation in a simple model of lithosphere–mantle flow with dynamic self-lubrication

David Bercovici *

Department of Geology and Geophysics, School of Ocean and Earth Science and Technology, University of Hawaii, 2525 Correa Road, Honolulu, HI 96822, USA

Received 15 April 1996; accepted 17 July 1996

Abstract

One of the more enigmatic features of the Earth's style of mantle convection is plate tectonics itself, in particular the existence of strike-slip, or toroidal, motion. Toroidal motion is uncharacteristic of basic thermal convection, but necessarily forms through the interaction of convective flow and nonlinear rheological mechanisms. Recent studies have implied that the empirically determined power-law rheologies of mantle silicates are not sufficient to generate the requisite toroidal motion. A simple source–sink model of mantle or lithospheric flow shows that dynamic self-lubrication, which arises through the coupling of viscous heating and temperature-dependent viscosity, is highly successful at generating strike-slip motion. In particular, as the viscosity of the fluid system becomes more temperature dependent, the toroidal flow field makes an abrupt transition from a state of weak, unplate-like motion to a state with intense and extremely focused structure. In essence, the fluid dynamical model develops strike-slip faults.

Keywords: plate tectonics; plates; mantle; convection; viscosity; strike-slip faults

1. Introduction

1.1. The plate generation problem

Plate tectonics is generally recognized as the surface expression of thermal convection in the mantle–lithosphere system [1]. However, one of the most important yet elusive goals of geodynamics and tectonophysics is the self-consistent unification of the physical theories of plate tectonics and mantle convection. Efforts toward unification have generally been taken with two different approaches. The first

approach examines plate–mantle coupling; the second approach treats the plate generation problem itself. Plate–mantle coupling studies examine how mantle flow interacts with over-riding plates that have a given geometry [2–6] or with a lithosphere that has prescribed weak zones [7,8]. Plate generation studies investigate how the plates and plate margins themselves are naturally generated (i.e., as self-organizing structures) from the nonlinear dynamics of the mantle–lithosphere system [9–14].

One of the primary features of plate tectonics not readily generated by basic convective theory is toroidal or strike-slip motion. Toroidal motion accounts for a major portion of the Earth's surface

* Fax: +1 808 956 2538. E-mail: dberco@wai.soest.hawaii.edu

deformation [2,15–18] but is, in fact, essentially nonconvective. That is, it involves only horizontal flow and is thus not directly driven by buoyancy forces and does not transport heat or mass out of the Earth's interior. Without toroidal flow, motion at the Earth's surface would be entirely unplate-like; that is, it would appear like the top of a simple convecting fluid, with only convergent and divergent features, no strike-slip margins and broadly distributed deformation. In short, toroidal motion is an integral feature of the plate-like behavior of the Earth's surface and thus knowledge of how toroidal motion is excited in the mantle–lithosphere system is key to understanding how plates are generated. (It is important to note that toroidal motion cannot be explained as being caused by the plates; this is a tautology equivalent to claiming that plate-like motion is due to the existence of plates).

1.2. Dynamic self-lubrication

The most fundamental clue as to the origin of toroidal flow is that, in highly viscous media such as the mantle, toroidal motion can only arise through the coupling of basic convective flow (called poloidal motion, which involves upwellings, downwellings and divergent/convergent motion at the surface) with a spatially variable viscosity [9,12,13,19,20]. (To a large extent, the fluid model of the mantle–lithosphere system is the simplest possible paradigm for describing irrecoverable deformation; this model only crudely represents nonfluid behavior at plate margins, such as brittle failure, through spatial and temporal averaging). The standard silicate viscosity is indeed variable by virtue of temperature, pressure and stress dependence. However, this rheology appears to permit very little toroidal motion in basic Boussinesq (nearly incompressible) convection [19,21]. It has already been shown [12,13] that, in simple models of lithosphere–mantle flow, plate-like toroidal motion is best obtained with a self-lubricating stick–slip rheology (wherein both the fluid viscosity and the very resistance to flow itself decrease with increasing deformation rate). Although the stick–slip rheology is purely hypothetical, it is based on the feedback between frictional heating and thermoviscous behavior (i.e., temperature-dependent vis-

cosity) [22]. The essence of such a feedback mechanism is that as the medium is deformed more rapidly it becomes hotter and weaker, and thus more readily deformed [23]. The stick–slip rheology itself approximates this feedback mechanism through a stress–strain-rate constitutive law but, in so doing, assumes all processes are one-dimensional (1-D) and steady state; that is, 1-D conductive heat loss instantaneously removes frictional heating [22]. We therefore refer to the stick–slip rheology as *simple self-lubrication*. When heat transport is rigorously accounted for, with three-dimensionality, nonlinear advection and time dependence, the feedback mechanism has even greater potential for generating rich, complex behavior; in this case we refer to the feedback mechanism as *dynamic self-lubrication*.

As with simple self-lubrication, the more physically rigorous and self-consistent dynamic self-lubrication is likely to play an important role in the generation of plate-like toroidal motion. Dynamic self-lubrication in non-Boussinesq convection has been found to lead to a variety of important phenomena [24–27] and, in particular, as shown by Balachandar et al. [28], to enhance the generation of toroidal motion in three-dimensional flows. Indeed, Bercovici [14] proposed that the purpose of the seemingly superfluous toroidal motion is closely tied to the generation of viscous dissipation, a key ingredient of dynamic self-lubrication. These various studies all suggest that the extremely fundamental process of dynamic self-lubrication (i.e., the feedback between viscous heating and thermoviscous behavior), plays an important role in the generation of plate-like flows.

In this paper, we demonstrate that a simple model of mantle–lithosphere flow with dynamic self-lubrication leads to more plate tectonic-like toroidal motion than in any other fluid dynamical model to date. In this model, convective (poloidal) motion is prescribed by driving lithospheric surface flow with sources and sinks (analogous to ridges and subduction zones, respectively); toroidal motion arises from the interaction between this poloidal flow and dynamic self-lubrication. We are most concerned with the fundamental structure and origin of strike-slip plate margins, and not the overall plate geometries themselves; thus a very simple source–sink geometry is used to focus on the basic physics.

2. Theory

We drive purely two-dimensional horizontal flow in a thin, incompressible viscous layer with a simple source–sink field [12,13]. The fluid motion generates viscous heating which leads to temperature anomalies and thus a laterally heterogeneous viscosity field (since the fluid viscosity is temperature dependent). The coupling between viscosity gradients and the divergent/convergent flow provides a source for toroidal (strike-slip) motion. Here we briefly present the essential *dimensionless* equations of the theory and defer to Bercovici [12,13] and the Appendices for a more complete discussion.

Horizontal two-dimensional flow in cartesian coordinates is represented by the horizontal velocity vector:

$$\mathbf{v}_h = \nabla_h \phi + \nabla_h \times (\psi \hat{z}) \quad (1)$$

where ∇_h is the horizontal gradient, ϕ is the poloidal scalar potential, ψ is the toroidal stream function, and \hat{z} is the unit vector in the vertical direction. The source–sink field is simply a prescribed horizontal divergence which yields an equation for ϕ :

$$\nabla_h \cdot \mathbf{v}_h = \nabla_h^2 \phi = \frac{Pe}{\delta} S(x, y) \quad (2)$$

where Pe is the Peclet number, which here determines the velocity of the source–sink flow (see Appendix B and Appendix E), δ is the half-width of either the source or sink (see Appendix B), and $S(x, y)$ is a function which defines the shape of the source–sink field (see Appendix B and the top frame of Fig. 1). The stream function, ψ , is found through the equation of motion for shallow-layer creeping flow with variable viscosity; as shown in [12] this leads to:

$$\begin{aligned} & \mu \nabla_h^4 \psi + 2 \nabla_h \mu \cdot \nabla_h \nabla_h^2 \psi + \Delta^* \mu \Delta^* \psi + 4 \frac{\partial^2 \mu}{\partial x \partial y} \frac{\partial^2 \psi}{\partial x \partial y} \\ & = \hat{z} \cdot \nabla_h \mu \times \nabla_h \nabla_h^2 \phi + 2 \Delta^* \mu \frac{\partial^2 \mu}{\partial x \partial y} - 2 \frac{\partial^2 \mu}{\partial x \partial y} \Delta^* \phi \end{aligned} \quad (3)$$

where μ is the temperature-dependent viscosity and $\Delta^* = (\partial^2)/(\partial x^2) - (\partial^2)/(\partial y^2)$. For the sake of simplicity, and to display the minimum possible level of

nonlinearity and complexity in the fluid system, we use a linear dependence of viscosity on temperature (see Appendix C):

$$\mu(\Theta) = 1 - \nu \Theta \quad (4)$$

where ν controls the degree of temperature dependence (see Appendix E) and Θ is the temperature anomaly. The evolution of Θ is governed by a simple transport law with viscous dissipation (see Appendix D):

$$\frac{\partial \Theta}{\partial t} + \mathbf{v}_h \cdot \nabla_h \Theta = -\Theta + \nabla_h^2 \Theta + \mu(\Theta) \dot{\epsilon}^2 \quad (5)$$

where $\dot{\epsilon}^2$ is the second strain-rate invariant (see [12] and Appendix D).

Note that Θ is the temperature anomaly above the background temperature field of the model lithosphere; it therefore does not represent the total temperature one might observe (see Appendix D). Moreover, the temperature anomalies are very small in magnitude when the fluid viscosity is highly temperature dependent. This result is found a posteriori in the numerical experiments, but can also be seen by a simple scaling analysis of Eq. (5). Such an analysis shows that:

$$\Theta_{\max} \sim \frac{\dot{\epsilon}_{\max}^2}{1/\tau + \nu \dot{\epsilon}_{\max}^2} \quad (6)$$

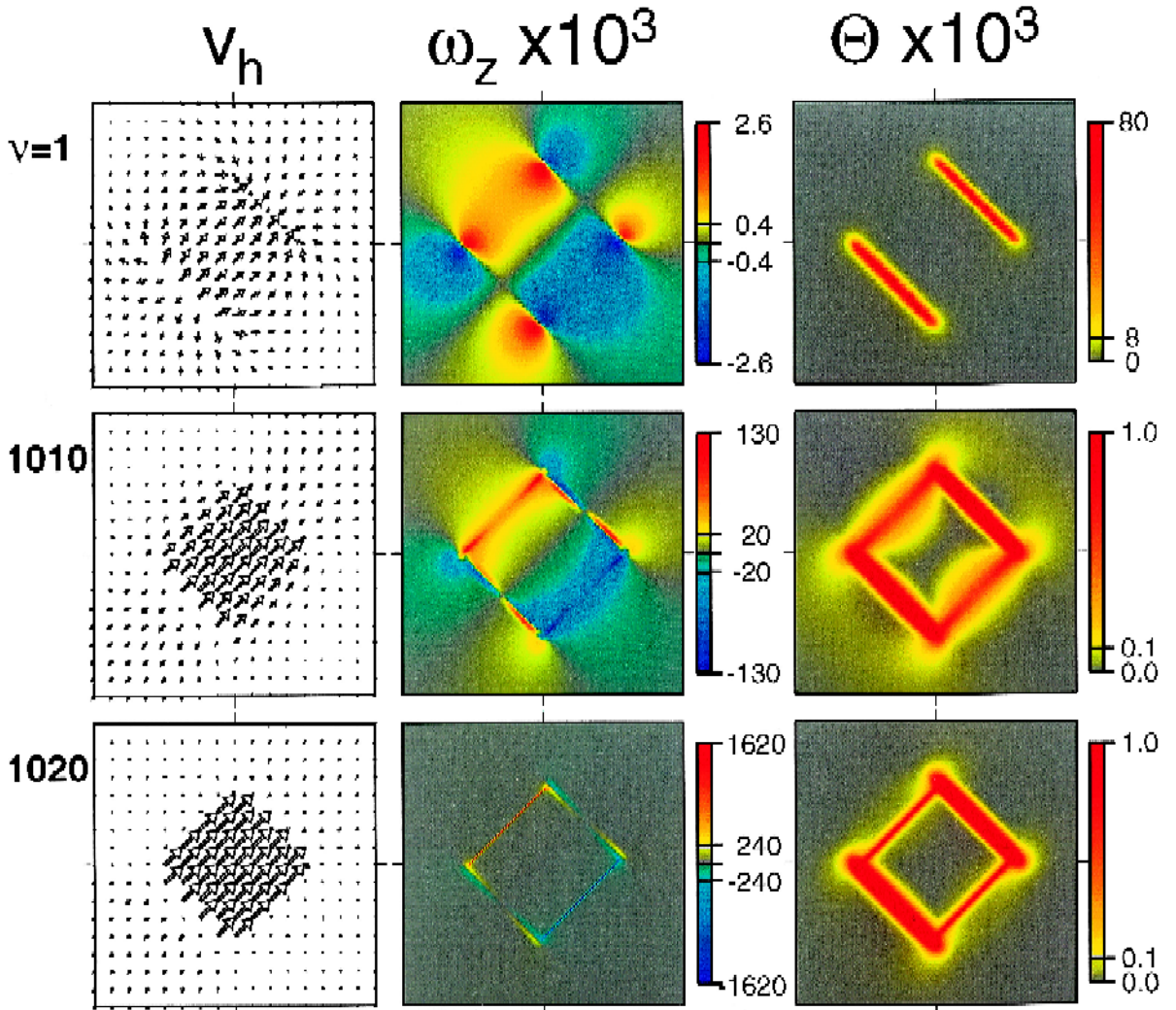
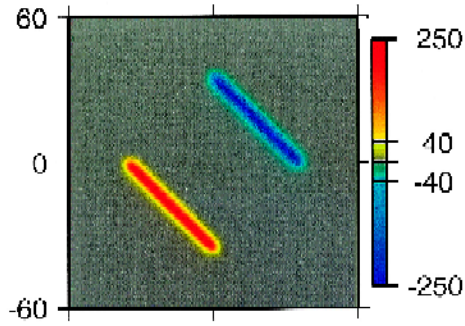
where the subscript *max* indicates maximum value and τ is the harmonic average of the dimensionless secular, advective and diffusive time scales for heat transport. Thus, a very large ν will induce a very small Θ_{\max} .

The governing equations for our system are Eq. (2), Eq. (3), Eq. (4) and Eq. (5). These are solved by a basic spectral-transform method; see Appendix F and [12,13,28].

3. Numerical experiments

The behavior described by this simple model is in fact quite dynamic and variable, displaying bifurcations of steady states, and time-dependent solutions. Here, we only report selected steady solutions which show the onset of plate-like (i.e., intense and focused) toroidal motion. Moreover, we use a source–

$(Pe/\delta) S \times 10^3$



sink field that, if perfect strike-slip margins formed, would yield a simple square plate [29]. Plate-like motion in this simple model is indicated by the following:

1. A toroidal-to-poloidal kinetic energy ratio:

$$KE_T/KE_P = \frac{\int_A \nabla_h \psi \cdot \nabla_h \psi dx dy}{\int_A \nabla_h \phi \cdot \nabla_h \phi dx dy} \quad (7)$$

(where A is the area of the two-dimensional domain) that is of order unity, as with idealized square plates [29] and the Earth's present-day plate motions [2,16];

2. A rectangular field of parallel, equal-length velocity vectors, which represents nearly solid body motion of material from the source to the sink;
3. Narrow, intense bands of vertical vorticity:

$$\omega_z = \hat{z} \cdot \nabla_h \times \mathbf{v}_h = -\nabla_h^2 \psi \quad (8)$$

where ω_z is equivalent to the rate of strike-slip shear, thus its organization into narrow bands indicates the formation of thin strike-slip margins.

4. A uniform viscosity pseudo-plate surrounded by a contiguous lower viscosity margin. In the present model, this condition is equivalent to a relatively cool pseudo-plate surrounded by a contiguous, uniformly 'hot' margin (i.e., of higher temperature than the background thermal state).

The ranges of values for Pe and ν relevant for the Earth are approximately $1 \leq Pe \leq 100$ and $10 \leq \nu \leq 10^7$ (see Appendix G). Here, we use $Pe = 1$ and $\delta = 2$ (i.e., a source and sink each with a width that is 2/3 to 1/2 of the fluid layer thickness; see Appendix E) and determine the effect of making the viscosity increasingly temperature dependent (i.e., increasing ν) on the toroidal motion. For a given Pe ,

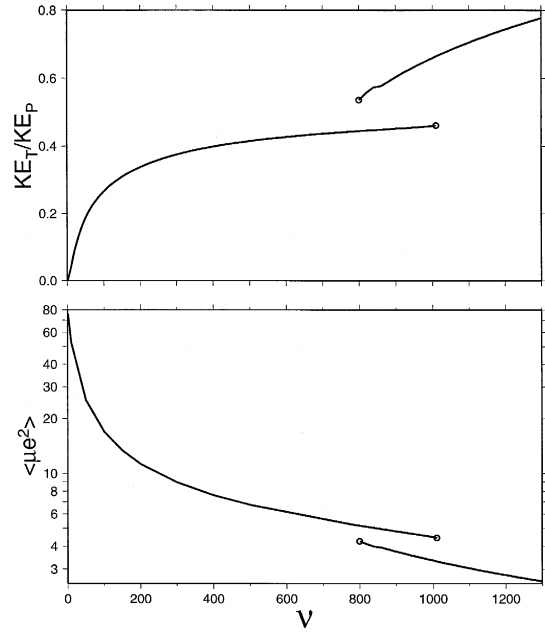


Fig. 2. Toroidal–poloidal kinetic energy ratio KE_T/KE_P and integrated viscous dissipation $\langle \mu \dot{\epsilon}^2 \rangle$ versus viscosity variability ν for flows driven by the source–sink field of Fig. 1. The bifurcation or transition points are indicated by circles. Bifurcation from the unplate-like branch to the plate-like one occurs at the right circle in each plot; the reverse bifurcation (with hysteresis) occurs at the left circle.

the poloidal field ϕ remains unchanged, regardless of ν .

For $\nu = 0$, toroidal motion does not exist, since viscosity would be constant; toroidal flow is in fact still very weak at $\nu = 1$ (Fig. 1). Toroidal motion and energy steadily grow with increasing ν (Fig. 1 and Fig. 2), yet the toroidal energy appears to saturate (i.e., approaches an asymptotic value) as $\nu \rightarrow 1010$. For the solutions with $\nu \leq 1010$ the toroidal

Fig. 1. Flow and temperature fields for selected steady state solutions discussed in the text. The source–sink field $(Pe/\delta)S(x, y)$ which drives the flow is shown in the top frame. Horizontal velocity \mathbf{v}_h (left column), vertical vorticity (or rate of strike-slip shear) ω_z (middle column), and temperature Θ (right column) are shown for three values of the viscosity variability (indicated at the far left), i.e., one low value of ν , and two values of ν on either side of the transition or bifurcation from the unplate-like solutions to plate-like ones. The minimum and maximum dimensionless values (multiplied by 10^3) of each scalar field are shown on the color scales which are stretched to emphasize nonzero values. Note that positive vorticity represents counter-clockwise rotation or left-lateral strike-slip shear; negative vorticity is right-lateral strike-slip shear. The maximum velocity vector length represents a dimensionless speed of 0.94, which is 94% of the speed of the original idealized plate from which the source-sink field was derived (see Appendix E). Although the calculation domain was $-100 \leq x, y \leq 100$, only the domain within $-60 \leq x, y \leq 60$ is shown (given that the remaining domain contains little or no activity). See also Appendix F for discussion of the numerical solutions.

energy is significant, but the actual toroidal fields are relatively diffuse and unplate-like. Moreover, the temperature anomalies Θ are most concentrated over the source and sink, and more diffuse over the strike-slip zones (Fig. 1).

At $\nu \approx 1020$, a bifurcation occurs to a different branch of solutions (Fig. 2) which persists to higher ν . The high and low ν branches display hysteresis (i.e., they overlap for a finite range of ν) which is characteristic of cubically nonlinear systems, such as our model equations. Most importantly, the bifurcation at $\nu = 1020$ marks a dramatic change in the structure of the toroidal and temperature fields. At this transition, the toroidal kinetic energy jumps by almost 50%, and the velocity field becomes much more plate-like (i.e., it becomes a rectangular patch of parallel vectors). The temperature anomalies are as highly (if not more) concentrated around the strike-slip margins as around the source and sink; this yields the desired plate-like viscosity distribution (i.e., a uniform, high viscosity plate interior, and narrow, contiguous, lower viscosity margins).

By far the most remarkable features of the transition at $\nu = 1020$ are: (1) the vorticity or strike-slip shear becomes focused into extremely narrow bands; and (2) the maximum vorticity appears to increase by more than 1000%. The regions of concentrated vorticity for the solution with $\nu = 1020$, indeed, have many of the properties of singularities (see Appendix F). Although the actual numerical values of the maximum vorticity must, therefore, be interpreted with caution (Appendix F), such behavior also suggests that the numerical model is attempting to generate discontinuous plate motion. In essence, the transition at $\nu = 1020$ marks the formation of a strike-slip fault in a fluid dynamical system.

4. Discussion and conclusions

In this paper we have used a very simple model to demonstrate that plate-like toroidal motion can be generated from convective-type (poloidal) flow using only basic first principles fluid mechanics and thermodynamics. In particular, dynamic self-lubrication (i.e., the feedback between viscous heating and the temperature dependence of viscosity) is shown to yield a virtual transform fault in a fluid. However,

this pseudo-fault occurs only after a bifurcation or transition to a state with fairly high viscosity contrasts between cold and hot fluid. These viscosity contrasts are on the order of 1000, which are well within reason for Earth-like conditions.

The cause for the transition to plate-like motion probably lies in the basic thermodynamics of the overall system. In particular, the surface integrated viscous heating $\langle \mu \dot{\epsilon}^2 \rangle$ not only decreases as the toroidal energy rises, but it drops by a considerable fraction across the transition to the highly plate-like state (Fig. 2). The jump to plate-like motion therefore appears to occur to lessen the net dissipation of the mechanical work that is done by the convective flow in moving material from the source to the sink (see [14] for more discussion about the reduction of viscous heating by plate-like toroidal flow).

Although the relatively cold temperatures of the Earth's surface (especially the sea floor) and high lithospheric viscosities are likely to put the Earth on the high ν , plate-like side of the transition (see Appendix G), the hotter temperatures and thus lower lithospheric viscosities of planets such as Venus or the ancient Earth might place these bodies on the low ν , unplate-like side of the transition. Although these inferences are based on a very simple model, the theory presented here may provide some insight into some of the differences between the tectonic states of the present-day Earth and Venus or the ancient Earth.

Finally, given the suggested importance of dynamic self-lubrication and viscous heating for generating plate-like toroidal motion, it is worth addressing the observability of viscous heating at plate margins. Viscous dissipation is typically discounted as a negligible effect, mostly because there is no significant heat flow anomaly at transform faults where viscous heating would conceivably be greatest [30]. However, in the dynamic self-lubrication mechanism, viscosity μ necessarily decreases as deformation rate $\dot{\epsilon}^2$ increases, and these competing effects counteract each other's contribution to viscous heating. This balance in fact causes the maximum dissipation $\max(\mu \dot{\epsilon}^2)$ and thus the maximum temperature anomaly Θ_{\max} to reach asymptotic limits of $(\tau\nu)^{-1}$ and ν^{-1} , respectively, as $\dot{\epsilon}_{\max}^2$ becomes sufficiently large (see Eq. (6)). For fluids with strongly temperature dependent viscosity (large ν) the asymp-

otic limits on temperature and heat production are therefore very small. This can be understood physically by considering that, for a given strain rate, as viscous heating generates a thermal anomaly in an initially isothermal system, the viscosity over the deforming zone will decrease rapidly, causing the viscous heating to decrease as well. For large ν the maximum temperature will only reach a very small value before the viscosity is so reduced that the subsequently diminished viscous heating can be balanced by thermal diffusion and other transport phenomenon. Thus, for large strain rates and strongly temperature-dependent viscosity, viscous heating and associated temperature anomalies are very small in magnitude (see also Fig. 1 and Appendix G). Therefore, the temperature and heat flow anomalies due solely to viscous dissipation would be undetectable in the background of lithospheric and mantle heat flow (Appendix G), in agreement with the observation that heat flow at transform faults is negligible [30].

Although our model is quite simple and idealized, it demonstrates that a virtual strike-slip fault with negligible heat flow can be generated in a fluid dynamical system. Though more realistic models are clearly warranted, the work presented here suggests that dynamic self-lubrication may be a fundamental ingredient for the generation of plate tectonics from mantle convection.

Acknowledgements

The author thanks Stuart Weinstein, David Yuen and an anonymous reviewer for helpful comments and/or discussions. This work was supported by NSF grant EAR-9458405. [RV]

Appendix A. Modeling considerations

As shown in Eq. (1), fluid velocity is separated into poloidal and toroidal parts. Poloidal flow is driven by a source–sink field and, as shown in Eq. (3), toroidal flow is driven by the coupling of poloidal motion to viscosity gradients. Nonzero viscosity gradients are caused by the viscosity's dependence on

temperature, and temperature anomalies are generated by viscous heating.

In the following appendices we first present the *dimensional* equations for the source–sink field and resulting poloidal field (Appendix B), the temperature-dependent viscosity (Appendix C), and the evolution of the temperature field (Appendix D); nondimensionalization of these equations is discussed in Appendix E. The equation governing the toroidal flow field has been discussed elsewhere [12]; in fact, Eq. (3) always appears the same, regardless of whether it is dimensional or nondimensional. We then outline the numerical methods used for solving the governing equations and discuss the quality and limitations of the numerical solutions (Appendix F). Finally, in Appendix G we evaluate the nondimensional control parameters for Earth-like conditions and discuss the associated value of the nondimensionalizing temperature scale (which determines the dimensional values of the thermal anomalies and resulting heat flow anomalies).

Appendix B. The source–sink field and poloidal flow

We derive a dimensional source–sink function from the motion of a square plate with sides of length 2α and margins of finite width 2δ (both presently with dimensional units). We employ an arbitrary coordinate system, denoted by (x', y') , and prescribe the plate to move at a dimensional speed V in the y' direction. Defining the coordinate origin at the plate's center, the velocity field of the plate as a function of x' and y' is thus $Vs(x')s(y')\hat{y}'$ where:

$$s(\zeta) = \frac{\tanh\left(\frac{\zeta + \alpha}{\delta}\right) - \tanh\left(\frac{\zeta - \alpha}{\delta}\right)}{2\tanh(\alpha/\delta)} \quad (9)$$

The source–sink function is simply the horizontal divergence of the plate's velocity; thus the horizontal divergence of the dimensional fluid velocity \mathbf{v}_h is:

$$\begin{aligned} \nabla_h \cdot \mathbf{v}_h &= \nabla_h^2 \phi = \nabla_h \cdot (Vs(x')s(y')\hat{y}') \\ &= \frac{V}{\delta} s(x')f(y') \end{aligned} \quad (10)$$

where:

$$f(\zeta) = \frac{\operatorname{sech}^2\left(\frac{\zeta + \alpha}{\delta}\right) - \operatorname{sech}^2\left(\frac{\zeta - \alpha}{\delta}\right)}{2 \tanh(\alpha/\delta)} \quad (11)$$

Eq. (10) therefore provides a governing equation for the dimensional poloidal potential ϕ . As in [12], the $x' - y'$ axes are rotated clockwise 45° relative to the $x - y$ frame of the numerical computations; that is, $(x', y') = (x - y, x + y)\sqrt{2}$. The rotation of the plate and hence the source–sink field is done to avoid roll-like flows caused by the periodic boundaries employed in the spectral-transform method (see Appendix F). Finally, we note that this source–sink field is chosen because it is derived from motion of a simple plate; we may thus determine if the application of our nonlinear theory can recover, in some form, the original plate.

Appendix C. Rheology

Our dimensional viscosity has the simplest possible temperature dependence:

$$\mu(T) = \mu_o(1 - \beta T) \quad (12)$$

where μ_o is the viscosity when the temperature anomaly is zero, and β governs the temperature dependence of the viscosity and has units of K^{-1} . With this rheology, we assume that temperature anomalies are relatively small (see Appendix G) and thus we linearize the Arrhenius law for silicate rheology.

Appendix D. The temperature equation

The dimensional temperature field, averaged across the thickness of the fluid layer, is governed by a simple advection–diffusion equation forced by viscous heating:

$$\frac{\partial T}{\partial t} + \mathbf{v}_h \cdot \nabla_h T = -\frac{C\kappa}{H^2} T + \kappa \nabla_h^2 T + \frac{2\mu}{\rho c_p} \dot{\epsilon}^2 \quad (13)$$

where T is the temperature anomaly due to viscous heating; κ is thermal diffusivity; H is the thickness

of the fluid layer; ρ is fluid density; c_p is heat capacity; C is a nondimensional constant, and

$$\dot{\epsilon}^2 = 2 \left[\left(\frac{\partial^2 \phi}{\partial x^2} + \frac{\partial^2 \psi}{\partial x \partial y} \right)^2 + (\nabla_h^2 \phi)^2 - \nabla_h^2 \phi \left(\frac{\partial^2 \phi}{\partial x^2} + \frac{\partial^2 \psi}{\partial x \partial y} \right) \right] + \frac{1}{2} \left(2 \frac{\partial^2 \phi}{\partial x \partial y} - \Delta^* \psi \right)^2 \quad (14)$$

is the second strain-rate invariant [12]. The first term on the right of Eq. (13) accounts for diffusive loss through the bottom and/or top of the fluid layer; for example, if we assume that T is the vertically averaged temperature anomaly and that the actual profile is nearly parabolic or sinusoidal (to match conditions that T vanishes at the top and bottom of the layer), then C would be $O(10)$. The last term represents viscous dissipation. The above equation also implicitly accounts for the loss (or influx) of heat due to the ejection (injection) of viscously heated fluid out of (in to) the sink (source) region. It is important to note that T is the temperature anomaly above the background lithospheric temperature field, which we assume varies on a much broader spatial scale than does T itself. This assumption is only strictly valid far away from ridges and subduction zones, but is sufficiently acceptable given the simplicity of our model. Moreover, because the only source of heat for T is viscous dissipation, both the source (ridge) and sink (subduction zone) will appear ‘hot’, counter to our intuition that subduction zones are ‘cold’. We, in fact, find, a posteriori, that the temperature anomalies for strongly variable viscosity are quite small (see also Eq. (6) and Appendix G) and are thus unlikely to change significantly the background lithospheric temperature field (thus subduction zones would continue to appear ‘cold’ even with viscous heating, as expected).

Appendix E. Nondimensionalization

We nondimensionalize x , y , α and δ by H/\sqrt{C} (and thus ∇_h by \sqrt{C}/H), time t by $(H^2)/(C\kappa)$, ϕ

and ψ both by κ , \mathbf{v}_h by $(\sqrt{C}\kappa)/(H)$, and viscosity μ by μ_o . We also define a dimensionless temperature such that:

$$T = \frac{2C\mu_o\kappa}{\rho c_p H^2} \Theta \quad (15)$$

The dimensional Eq. (10), Eq. (12) and Eq. (13) become the dimensionless governing Eq. (2), Eq. (4) and Eq. (5), respectively, with control parameters:

$$\nu = \frac{2C\mu_o\kappa\beta}{\rho c_p H^2} \text{ and } Pe = \frac{VH}{\sqrt{C}\kappa} \quad (16)$$

(Note that this Peclet number is much smaller than what is typically used for mantle flow since it is based on lithospheric thickness instead of mantle thickness). Eq. (3), governing toroidal motion (see [12]), applies to both the dimensional and nondimensional formulations. In all calculations shown we use $Pe = 1$ and, for the source–sink field, $\alpha = 25$ and $\delta = 2$. Note that the dimensionless velocity of the original plate is $Pe = 1$; this velocity can be compared to the fluid velocity generated in our theoretical model (Fig. 1).

Appendix F. Numerical methods and solutions

The differential equations are solved by a spectral-transform technique. The nonlinear products in each equation are calculated on an $x - y$ grid, and these products are Fourier transformed to a spectral or wave-number domain. These transformed nonlinear terms are then used as forcing functions for the fourier-transformed linear parts of the relevant equations. Time integration is performed by basic finite differencing. The calculation domain is $-100 \leq x, y \leq 100$. See [28] and [12] for examples.

The steady numerical solutions presented in this paper are all for $Pe = 1$ and a wide range of ν . The branches of steady solutions represented in Fig. 2 were all found by using the steady solution at a particular ν as an initial condition for a solution at a neighboring value of ν . In this way we marched up or down in ν to map out the steady solutions. The bifurcation at $\nu = 1020$ occurred while marching upward on the low ν branch; the reverse bifurcation at $\nu = 800$ was obtained while marching down on the high ν branch. The solutions on the low ν un-

plate-like branch were obtained on a 512×512 grid; convergence tests indicate that the solutions shown do not change at all for grids with resolution finer than on a 256×256 grid. The solutions on the high ν plate-like branch were done with grids up to 1024×1024 resolution. The values of the kinetic energy ratio and net viscous dissipation shown in Fig. 2 were obtained from solutions on a 512×512 grid. The solution for $\nu = 1020$ shown in Fig. 1 was obtained on a 1024×1024 grid. Convergence tests for the plate-like solutions show that global quantities (such as average kinetic and thermal energy, and net viscous heating), and the temperature and velocity fields do not change significantly for grids finer than a 384×384 grid. The contiguous and highly focused structure of the vorticity concentrations also remains qualitatively robust and unchanged for grids finer than a 256×256 grid. However, the vorticity concentrations for the plate-like solutions behave remarkably like singularities in that the maximum value of the vorticity does not converge, even up to 1024×1024 grids. As one might expect from a singularity, the maximum vorticity scales almost exactly with an increase in the resolution; for example, as the grid resolution is moved from 512×512 to 1024×1024 the maximum vorticity almost exactly doubles. Therefore, although it is very intriguing that the fluid dynamical system appears to be generating singularities in the vorticity field (which one desires in order to obtain ideal plate-like motion), the maximum values of vorticity for the $\nu = 1020$ solution (Fig. 1) must be interpreted with caution.

Appendix G. Nondimensional parameter values and the temperature scale

Earth-like ranges for Pe and ν (i.e., $1 \leq Pe \leq 100$ and $10 \leq \nu \leq 10^7$) are estimated using $C \approx 10$, $\kappa = 10^{-6} \text{ m}^2/\text{s}$, $\rho = 3000 \text{ kg}/\text{m}^3$, and $c_p = 1000 \text{ J}/\text{kg}/\text{K}$. For more poorly constrained dimensional quantities we use $10 \text{ km} \leq H \leq 100 \text{ km}$ for lithospheric thickness and $1 \text{ cm}/\text{yr} \leq V \leq 10 \text{ cm}/\text{yr}$ for plate velocity. There are few bounds on ambient lithospheric viscosity; thus to be safe we use $10^{24} \text{ Pa s} \leq \mu_o \leq 10^{27} \text{ Pa s}$, which contains empirical estimates of 10^{25} Pa s , based on sedimentary basin

subsidence [31,32]. Estimates of β from Eq. (12) are derived using the simple silicate rheological law:

$$\mu = \mu_o e^{\frac{\alpha T_m}{T_o} \left(\frac{1}{1+T/T_o} - 1 \right)} \quad (17)$$

where T_m is the melting temperature, for which we use a typical surficial value of 2000 K; moreover, $\alpha \approx 30$, and the lithospheric background temperature is in the range of $300 \text{ K} \leq T_o \leq 1000 \text{ K}$ (see [33]). If $T \ll T_o$, then $\mu \approx \mu_o(1 - \beta T)$ where $\beta = \alpha T_m / T_o^2$; thus the values of β lie in the range $0.06 \text{ K}^{-1} \leq \beta \leq 0.7 \text{ K}^{-1}$. The temperature scale from Eq. (15) is in fact simply ν/β . For the largest ν used, the temperature scale lies between 1000 K and 20,000 K. However, the maximum nondimensional temperature anomaly Θ_{\max} is approximately 10^{-3} (see Fig. 1), thus the dimensional thermal anomaly is small (i.e., between 1 K and 20 K). (These small thermal anomalies can generate large viscosity contrasts because, at the relatively cold temperatures of the lithosphere, viscosity is much more sensitive to changes in temperature than it would be in the deeper mantle; see Eq. (17)). The resulting maximum heat flow anomaly is thus approximately $\rho c_p \kappa \nu \Theta_{\max} / (\beta H)$ which (given the ranges in H and ν/β) lies between 0.03 and 6 mW/m², that is, 20–3000 times smaller than the background seafloor heat flow of approximately 100 mW/m² [33].

References

- [1] D. Forsyth and S. Uyeda, On the relative importance of the driving forces of plate motion, *Geophys. J. R. Astron. Soc.* 43, 163–200, 1975.
- [2] B.H. Hager and R.J. O'Connell, Subduction zone dip angles and flow driven by plate motion, *Tectonophysics* 50, 111–133, 1978.
- [3] B.H. Hager and R.J. O'Connell, Kinematic models of large-scale flow in the Earth's mantle, *J. Geophys. Res.* 84, 1031–1048, 1979.
- [4] B.H. Hager and R.J. O'Connell, A simple global model of plate dynamics and mantle convection, *J. Geophys. Res.* 86, 4843–4867, 1981.
- [5] L. Cserepes and U. Christensen, Three-dimensional convection under drifting plates, *Geophys. Res. Lett.* 17, 1497–1500, 1990.
- [6] C.W. Gable, R.J. O'Connell and B.J. Travis, Convection in three dimensions with surface plates: Generation of toroidal flow, *J. Geophys. Res.* 96, 8391–8405, 1991.
- [7] S. Zhong and M. Gurnis, Mantle convection with plates and mobile, faulted plate margins, *Science* 267, 838–843, 1995.
- [8] S. Zhong and M. Gurnis, Towards a realistic simulation of plate margins in mantle convection, *Geophys. Res. Lett.* 22, 981–984, 1995.
- [9] N.M. Ribe, The dynamics of thin shells with variable viscosity and the origin of toroidal flow in the mantle, *Geophys. J. Int.* 110, 537–552, 1992.
- [10] S. Weinstein and P. Olson, Thermal convection with non-Newtonian plates, *Pure Appl. Geophys.* 146, 1996.
- [11] S. Weinstein, Thermal convection in a cylindrical annulus with a non-Newtonian outer surface, *Proc. IUTAM Symp. on Mechanical Problems in Geodynamics*, Beijing, China, *Pure Appl. Geophys.*, in press.
- [12] D. Bercovici, A simple model of plate generation from mantle flow, *Geophys. J. Int.* 114, 635–650, 1993.
- [13] D. Bercovici, A source–sink model of the generation of plate tectonics from non-Newtonian mantle flow, *J. Geophys. Res.* 100, 2013–2030, 1995.
- [14] D. Bercovici, On the purpose of toroidal flow in a convecting mantle, *Geophys. Res. Lett.* 22, 3107–3110, 1995.
- [15] A.M. Forte and W.R. Peltier, Plate tectonics and aspherical earth structure: The importance of poloidal–toroidal coupling, *J. Geophys. Res.* 92, 3645–3679, 1987.
- [16] R.J. O'Connell, C.W. Gable and B.H. Hager, Toroidal–poloidal partitioning of lithospheric plate motion, in: *Glacial Isostasy, Sea Level and Mantle Rheology*, R. Sabadini et al., eds., pp. 535–551, Kluwer Academic, Norwell, Mass., 1991.
- [17] O. Cadek and Y. Ricard, Toroidal/poloidal energy partitioning and global lithospheric rotation during Cenozoic time, *Earth Planet. Sci. Lett.* 109, 621–632, 1992.
- [18] C. Lithgow-Bertelloni, M.A. Richards, Y. Ricard, R.J. O'Connell and D.C. Engebretson, Toroidal–poloidal partitioning of plate motions since 120 Ma, *Geophys. Res. Lett.* 20, 375–378, 1993.
- [19] U. Christensen and H. Harder, Three-dimensional convection with variable viscosity, *Geophys. J. Int.* 104, 213–226, 1991.
- [20] O. Cadek, Y. Ricard, Z. Martinec and C. Matyska, Comparison between Newtonian and non-Newtonian flow driven by internal loads, *Geophys. J. Int.* 112, 103–114, 1993.
- [21] M. Ogawa, G. Schubert and A. Zebib, Numerical simulations of three-dimensional thermal convection in a fluid with strongly temperature-dependent viscosity, *J. Fluid Mech.* 233, 299–328, 1991.
- [22] J.A. Whitehead and R.F. Gans, A new, theoretically tractable earthquake model, *Geophys. J. R. Astron. Soc.* 39, 11–28, 1974.
- [23] G. Schubert and D.L. Turcotte, One-dimensional model of shallow mantle convection, *J. Geophys. Res.* 77, 945–951, 1972.
- [24] S. Balachandar, D.A. Yuen, D.M. Reuteler and G.S. Lauer, Viscous dissipation in 3-dimensional convection with temperature-dependent viscosity, *Science* 267, 1150–1153, 1995.
- [25] P.J. Tackley, Effects of strongly variable viscosity on three-dimensional compressible convection in planetary mantles, *J. Geophys. Res.* 101, 3311–3332, 1996.

- [26] T.B. Larsen, D.A. Yuen and A.V. Malevsky, Dynamical consequences on fast subducting slabs from a self-regulating mechanism due to viscous heating in variable viscosity convection, *Geophys. Res. Lett.* 22, 1277–1280, 1995.
- [27] T.B. Larsen, D.A. Yuen, J.L. Smedso and A.V. Malevsky, Thermomechanical modeling of pulsation tectonics and consequences on lithospheric dynamics, *Geophys. Res. Lett.* 23, 217–220, 1996.
- [28] S. Balachandar, D.A. Yuen and D.M. Reuteler, Localization of toroidal motion and shear heating in 3-D high Rayleigh number convection with temperature-dependent viscosity, *Geophys. Res. Lett.* 22, 477–480, 1995.
- [29] P. Olson and D. Bercovici, On the equipartitioning of kinetic energy in plate tectonics, *Geophys. Res. Lett.* 18, 1751–1754, 1991.
- [30] A.H. Lachenbruch and J.H. Sass, Heat flow and energetics of the San Andreas fault zone, USGS Open File Rep. 80-625, pp. 47–146, 1980.
- [31] C. Beaumont, The evolution of sedimentary basins on a viscoelastic lithosphere, *Geophys. J. R. Astron. Soc.* 55, 471–497, 1976.
- [32] A.B. Watts, G.D. Karner and M.S. Steckler, Lithospheric flexure and the evolution of sedimentary basins, *Philos. Trans. R. Soc. London Ser. A* 305, 249–281, 1982.
- [33] D.L. Turcotte and G. Schubert, *Geodynamics: Applications of Continuum Physics to Geological Problems*, Wiley, New York, 1982.